

Lymphoma Neoplasm Computable scrutiny of Multi images on Gaussian Dissemination for INU

Dr.E.Gajendran¹, Dr.J.Vignesh²,Dr. K.P.Yadav³

¹Assistant Professor, Dept of CSE , Oxford College of Engineering,Tamilnadu, India,

²Assistant Professor, Dept of CSE, Oxford College of Engineering,Tamilnadu, India,

³Professor and Director, MIET, Greater Noida, Uttar Pradesh,India.

Abstract— In this paper, Intensity inhomogeneity causes considerable difficulty in the quantitative analysis of magnetic resonance (MR) images. Thus bias field estimation is a necessary pre-processing step before quantitative analysis of MR data. This paper presents a variational level set approach for bias correction and segmentation for images with intensity inhomogeneities. Our method is based on the observation that local intensity variations in relatively smaller regions are separable, despite the inseparability of the whole image. In the beginning we define a function for clustering the image pixels in a smaller neighborhood. The cluster centers in this objective function have a multiplicative factor that estimates the bias within the neighborhood. Generally the local intensity variations are described by the Gaussian distributions with different means and variances. In this work the objective functions are integrated over the entire domain with local Gaussian distribution of fitting energy, ultimately analyzing the data with a level set framework. Our method is able to capture bias of quite general profiles. Moreover, our model can also distinguish regions with similar intensity distribution with different variances. The proposed method has been rigorously validated with images acquired on variety of imaging modalities with promising results.

Keywords—: Bias Field, Level set, Atlas Registration, MRI, pattern recognition and brain tumor.

I. INTRODUCTION

In Lymphomas typically develop in the subcortical and subependymal white matter. Within the brain substance, the irregular tumor edge extends along perivascular spaces. The

spinal cord is frequently affected in secondary lymphoma. Lymphoma tumors are often multiple with central necrosis

in AIDS. Tumor lesions can cross the midline and may appear as a butterfly tumor involving both cerebral hemispheres. Involvement of the perivascular spaces with contrast enhancement or of the corpus callosum (glioma or metastatic neoplasm must be differentiated) is strongly suggestive of CNS lymphoma [Plotkin and Batchelor, 2001]. The classic appearance of lymphoma is an hypointense nodule or mass on T1-weighted images and hyperintense on corresponding T2-weighted images. On contrast enhanced T1-weighted MRI, lymphoma tends to enhance intensely and diffusely. A ring like enhancing pattern is seen most often in patients with AIDS (Figure 1.15). Of-ten, little or no surrounding vasogenic edema is demonstrated [Plotkin and Batchelor, 2001], [Wen et al., 2001].

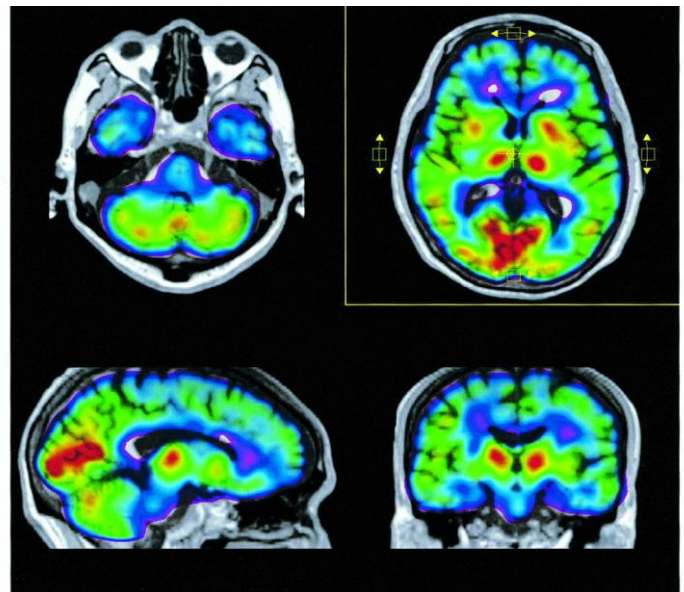


Fig 1.1 Lymphoma in PET Scan Image

The image processing is any form of signal processing for which the input is an image, such as a photograph or video frame; the output of image processing may be either an image or a set of characteristics or parameters related to the image. Most image-processing techniques involve treating the image as a two-dimensional signal and applying standard signal-processing techniques to it. Image processing usually refers to digital image processing, but optical and analog image processing also are possible. This article is about general techniques that apply to all of them. The acquisition of images (producing the input image in the first place) is referred to as imaging. Lymphoma is a type of blood cancer that occurs when B or T lymphocytes,[1] the white blood cells that form a part of the immune system and help protect the body from infection and disease, divide faster than normal cells or live longer than they are supposed to. Lymphoma may develop in the lymph nodes, spleen, bone marrow, blood or other organs[2] and eventually they form a tumor.[1]. Typically, lymphoma presents as a solid tumor of lymphoid cells. Treatment might involve chemotherapy and in some cases radiotherapy and/or bone marrow transplantation, and lymphomas can be curable depending on the histology, type, and stage of the disease.[3] These malignant cells often originate in lymph nodes, presenting as an enlargement of the node (a tumor). It can also affect other organs in which case it is referred to as extranodal lymphoma. Extranodal sites include the skin, brain, bowels and bone. Lymphomas are closely related to lymphoid leukemias, which also originate in lymphocytes but typically involve only circulating blood and the bone marrow (where blood cells are generated in a process termed haematopoiesis) and do not usually form static tumors.[3] There are many types of lymphomas, and in turn, lymphomas are a part of the broad group of diseases called hematological neoplasms. Hodgkin's lymphoma is one of the most well-known types of lymphoma,[30] and differs from other forms of lymphoma in its prognosis and several pathological characteristics. A division into Hodgkin's and non-Hodgkin's lymphomas is used in several formal classification symptoms. A Hodgkin's lymphoma refers to a lymphoma that has a specific type of cell visible when a biopsy is viewed under a microscope. Many low-grade lymphomas remain indolent for many years. In these lymphomas, metastases are very likely. For this reason, treatment of the non-symptomatic patient is often avoided. In these forms of lymphoma, watchful waiting is often the initial course of action. This is carried out because the harms and risks of treatment outweigh the benefits.[19] If a low-grade lymphoma is becoming symptomatic, radiotherapy or

chemotherapy are the treatments of choice; although they do not cure the lymphoma, they can alleviate the symptoms, particularly painful lymphadenopathy. Patients with these types of lymphoma can live near-normal lifespans, but the disease is incurable. Significant research into the causes, prevalence, diagnosis, treatment, and prognosis of lymphoma is being performed. Hundreds of clinical trials are being planned or conducted at any given time.[28] Studies may focus on effective means of treatment, better ways of treating the disease, improving the quality of life for patients, or appropriate care in remission or after cures. In general, there are two types of lymphoma research: clinical or translational research and basic research. Clinical/translational research focuses on studying the disease in a defined and generally immediately patient-applicable way, such as testing a new drug in patients. By contrast, basic science research studies the disease process at a distance, such as seeing whether a suspected carcinogen can cause healthy cells to turn into lymphoma cells in the laboratory or how the DNA changes inside lymphoma cells as the disease progresses. The results from basic research studies are generally less immediately useful to patients with the disease.[29]. Lymphocytes are white blood cells that move throughout the body in a fluid called lymph. They are transported by a network of vessels that make up the lymphatic system, part of the immune system. The lymphatic system - whose job it is to fight infections or anything else that threatens the body - is also comprised of lymph nodes that exist throughout the body to filter the lymph that flows through them. The lymph nodes swell and tenderize when a large number of microbial organisms collect inside of them, indicating local infection. Image enhancement is refers to accentuation, or sharpening, of image features such as boundaries, or contrast to make a graphic display more useful for display & analysis. This process does not increase the inherent information content in data. It includes gray level & contrast manipulation, noise reduction, edge crispness and sharpening, filtering, interpolation and magnification, pseudo coloring, and so on. Contrast enhancement is a common operation in image processing. It's a useful method for processing scientific images such as X-Ray images or satellite images. And it is also useful to improve detail in photographs that are over or under-exposed. Many clinical and research applications of MR imaging rely on segmentation in order to delineate different intensity distributions in each image. Unfortunately, most tissue classification methods are hindered by various imaging artifacts such as noise and intensity inhomogeneities. Segmentation experiments presented. It illustrate that the major problem for brain MR image segmentation is not noise rather, intensity inhomogeneities,

also named as bias field. The observed MRI signal J is the product of the true signal I generated by the underlying anatomy and spatially varying field factor B , and an additive noise N [2]:

$$J = (I + N) \cdot B$$

Given the observed signal J , the problem is to estimate the true image I . A group of techniques often take the logarithmic transform of both sides

$$\log(J) = \log((I + N) \cdot B) = \log(I + N) + \log(B)$$

If we named $\log(J)$ with $\sim J$, $\log(I + N)$ with $\sim I$ and $\log B$ with $\sim B$, respectively. It can be written as $\sim J = \sim I + \sim B$. Some correction techniques rely on measuring the coil sensitivity functions. These approaches can correct for coil sensitivities but cannot correct for other sources of intensity inhomogeneities. Many image processing methods have been proposed to estimate the bias field directly from the image. A key observation is that the bias field is smooth and most methods rely on this fact. The smoothness of B can be assured in the frequency domain. These methods are attractive since there is no other assumption on I and B . However, most of them may lose edge information, making the bias results inaccurate. Based on the assumption that the bias field is smooth, it can be approximated by polynomial functions, discrete cosine transforms, or thin plates such as a constrained membrane. When higher degrees of freedom are added, those methods become more computationally demanding. Unfortunately, these higher order polynomial functions can lead to spurious artifacts when fitting a strongly varying bias field.

I. LITERATURE SURVEY

A probabilistic deformable model for the representation of multiple brain structures is described. The statistically learned deformable model represents the relative location of different anatomical surfaces in brain magnetic resonance images (MRIs) and accommodates their significant variability across different individuals. The surfaces of each anatomical structure are parameterized by the amplitudes of the vibration modes of a deformable spherical mesh. For a given MRI in the training set, a vector containing the largest vibration modes describing the different deformable surfaces is created. This paper describes a framework for automatic brain tumor segmentation from MR images. The detection of edema is done simultaneously with tumor segmentation, as the knowledge of the extent of edema is important for diagnosis,

planning, and treatment. Whereas many other tumor segmentation methods rely on the intensity enhancement produced by the gadolinium contrast agent in the T1-weighted image, the method proposed here does not require contrast enhanced image channels. The only required input for the segmentation procedure is the T2 MR image channel, but it can make use of any additional non-enhanced image channels for improved tissue segmentation. Acquisition of non-contrast agent cine cardiac magnetic resonance (CMR) gated images through the cardiac cycle is, at present, a well-established part of examining cardiac global function. However, regional quantification is less well established. We propose a new automated framework for analyzing the wall thickness and thickening function on these images that consists of three main steps. First, inner and outer wall borders are segmented from their surrounding tissues with a geometric deformable model guided by a special stochastic speed relationship. The latter accounts for Markov-Gibbs shape and appearance models of the object-of-interest and its background. In the second step, point-to-point correspondences between the inner and outer borders are found by solving the Laplace equation and provide initial estimates of the local wall thickness and the thickening function index. Finally, the effects of the segmentation error are reduced and a continuity analysis of the LV wall thickening is performed through iterative energy minimization using a generalized Gauss-Markov random field (GGMRF) image model. The framework was evaluated on 26 datasets from clinical cine CMR images that have been collected from patients with eleven independent studies, with chronic ischemic heart disease and heart damage. The performance evaluation of the proposed segmentation approach, based on the receiver operating characteristic (ROC) and Dice similarity coefficients (DSC) between manually drawn and automatically segmented contours, confirmed a high robustness

II. METHODOLOGY

3.1 EXISTING METHOD

Another common assumption is that the image consists of piecewise homogeneous regions. The number of tissue types is assumed known. Classification schemes can then be improved to estimate the bias field. Wells et al. [20] extended the framework of maximum likelihood classification to estimate the bias field, and this innovation led to many refinements. The fuzzy c-means algorithm has been modified to estimate the bias field. All of these techniques determine clusters in feature space. Due to the

high intensity inhomogeneities, clusters spread over large regions, thus increasing the sensitivity to initial conditions and local minima. Some researchers maximized the information content in I instead of segmenting the image into classes

3.2 DISADVANTAGES

Level set methods have been extensively used for image segmentation. These method cannot deal with images with **strong bias field**. Li et al. [27] and our previous work [19] improved level set methods to segment images while **estimating the bias field and obtain good** results. But these methods are only based on the local mean information and cannot obtain segmented objects with same means and different variance.

3.3 PROPOSED METHOD

In this paper, we will improve our previous work [19]. The work only considers the local mean information and cannot segment objects with different variances. A unique advantage of our method is that the smoothness of the **computed bias field is intrinsically ensured by the data term** in a variational formulation. Furthermore, our model is able to distinguish regions with similar intensity means but different variances, thereby allowing fully automated applications. The proposed method has been implemented on both synthetic and real images acquired using different modalities. The level set function f can be simply initialized as a binary step function, which takes a negative constant value λ_0 inside the region R_0 and a positive constant value c_0 outside it.

3.4 ADVANTAGES

Although the local mean intensities are close, the local intensity variances are distinct, which enable our method to extract object boundary precisely.

A) Application to MR images

It shows the result for a 3T MR cardiac image, which has obvious noise. With the effect of the noise, the PC model cannot obtain an accurate result, which is based on the local intensity means information too. With the effect of strong noise and weak edges, the LBF method cannot obtain accurate result. Using the same initialization, the

intermediate results of our method are presented. Compared to the PC model and LBF model, our method can delineate the boundary more precisely. It shows the result for a 3T bias corrupted MR cardiac image, which also has weak edges and the result of LBF model. Due to the low image contrast in the right side of the image, the LBF model failed to extract the whole object boundaries. The model can **segment while estimating the bias field**. However, the model only uses the local intensity means and cannot obtain accurate results. Interestingly, our method successfully extracts object boundaries which has the corrected image and the **estimated bias field**. We also evaluated the performance of the algorithm on a set of in vivo medical images with intensity inhomogeneity. In these vessel images, some vessel boundaries are quite weak. Our method successfully extracts the object boundaries for these images, respectively.

B) Application on real-world images

The original images and initial contours, and our approach are shown from the left column to the right column. Our method successfully extracts the object boundaries for these images. It presents the results for other two real-world images. The **first row shows the result of rice image** corrupted by intensity inhomogeneity. The original images and initial contours, the results for the LBF model, our **model and the estimated bias field are shown from the left column to the right column**. It can be seen that the new contours can emerge during the evolution to extract multiple object boundaries. The second row shows the results of an image which is corrupted by intensity inhomogeneity due to nonuniform illumination, often seen in camera images. Our method successfully extracts the object boundaries for these images.

C) Robustness of our method

We compared our method to Wells et al. [20] and Leemput et al. [7] on more than 100 simulated images obtained from **some of them corrupted with bias field without noise and the others with both**. The average coefficients of variance values for the two kinds of images are listed in Table 1. It can be seen that the **coefficient of variation (CV) values of our method are lower than those of Wells' and Leemput's methods**, which indicates that the bias corrected images obtained in our method are more homogeneous than those of the other two methods. It can be seen that the entropy of our method is lower than those of Wells and Leemput's methods, which indicates that the bias corrected images obtained in our method are more homogeneous than those

of the other two methods. Quantitative evaluation was performed by computing the coefficient of joint variations (CJV) [38] between gray (GM) and white matter (WM) of the brain, which were segmented in all images. CJV is computed from standard deviations s and mean values m of the voxel intensities belonging to the two matters

$$CJV(GM, WM) = \frac{\sigma(GM) + \sigma(WM)}{|\mu(WM) - \mu(GM)|}$$

IV. ATLAS REGISTRATION

The weights in the hidden node necessitated to be set consuming "training" data. Consequently, subjects were alienated into training and testing data sets. Out of the 69 subjects, 2 random patients and 2 random controls were plump for as "test data", however the rest of the data set was cast off for training. Training data were utilized to feed into the neural networks as inputs and then comprehending the output, the weights of the hidden nodes were premeditated using back propagation algorithm. 120 trials were maneuvered on the same Neural Network, selecting 65 subjects erratically every time for retraining and 4 persisting subjects for testing to find the meticulousness of Neural network prediction. The proposed method has been implemented on both synthetic and real images acquired using different modalities. The level set function f can be simply initialized as a binary step function, which takes a negative constant value \tilde{c}_0 inside the region R_0 and a positive constant value c_0 outside it. In this paper, we choose the same value $c_0 \approx 4$ as in. For the experiments in this paper, we set the parameters $s \approx 5$, $m \approx 1$, and $n \approx 0.001 \approx 2552$ for all the images on a trial basis. The object and background have the same intensity means but different variances. Using the initial contour, the intermediate results of the piecewise constant (PC) model is presented. It can be seen that the PC model, which assumes that an image consists of statistically homogeneous regions fails to extract the object boundary. In our previous method, the local intensity means of object and background are rather close and the local intensity variance information is not taken into account, which results in an inaccurate decision on object boundary. It shows the result of our model and the estimated bias field, respectively. Although the local mean intensities are close, the local intensity variances are distinct, which enable our method to extract object boundary precisely.

List of Modules

- 1) Image segmentation based on local means
- 2) Bias correction based on local means

- 3) Image segmentation based on local distribution
- 4) Bias correction based on local distribution
- 5) Energy minimization in level set framework
- 6) The gradient flow

Image segmentation based on local means

It is generally assumed that the bias field is smooth or slowly varying. Ideally, the intensity I of each tissue should take a specific value c_i , which represents the measured physical property. We assume that the image I and the bias field B have the two different properties, i.e., the bias field B is slowly varying over the entire image domain and the image intensity I is fairly constant within each class of tissue.

As mentioned previously, the measured data J in the whole image are not separable based on their intensity values. Our previous method is based on an observation that intensities in a relatively small region are separable. The method defined an objective function to classify the data in the neighborhood L_y into N clusters using a K-means clustering method:

$$\varepsilon_y = \sum_{i=1}^N \int_{L_y \cap \Omega_i} \omega(x-y) |\tilde{J}(x) - \tilde{B}(y) - c_i|^2 dx$$

Bias correction based on local means

The cluster values to be optimized, and it is a non-negative weighting function such that $\int_{L_y} R = 1$ and $L_x = 1$. r is the radius of L_y . In the method, the weighting function is chosen as the Gaussian kernel. The ultimate goal is to find an optimal set of partitions for the entire image domain O , the bias field B , and the constants c_i . The minimization of a single objective function ε_y for a point y does not accomplish this goal. The method minimizes ε_y for all the points y . This can be achieved by minimizing the integral of ε_y over O . Therefore, the energy is written as

$$\mathcal{E}_{means} = \int_O \left(\sum_{i=1}^N \int_{\Omega_i} \omega(x-y) |\tilde{J}(x) - \tilde{B}(y) - c_i|^2 dx \right) dy$$

Image segmentation based on local distribution

To effectively exploit information on local intensities, we need to characterize the distribution of local intensities via partition of neighborhood as in [19]. The neighborhood L_y can be segmented by using the framework of maximum a

posteriori probability be the posteriori probability of the subregions $O_i \setminus L_y$ given the gray values. According to the Bayes rules:

$$p(x \in \Omega_i \cap A_y | \tilde{I}(x)) = \frac{p(\tilde{I}(x) | x \in \Omega_i \cap A_y) p(x \in \Omega_i \cap A_y)}{p(\tilde{I}(x))}$$

Assuming that the pixels within each region are independent, the QO MAP can be achieved by finding the maximum of $N=1$. Taking a logarithm, the maximization can be converted to the minimization of the following energy:

$$\mathcal{E}'_y = \sum_{i=1}^N \int_{\Omega_i} -\omega(x-y) \log p_{i,y}(\tilde{I}(x)) dx$$

Bias correction based on local distribution

There are various approaches to model the probability densities P including a full Gaussian density [29], or nonparametric Parzen estimator [30]. Most image segmentation methods assume a global model for the probability of each region. As we know, there exist quite a few spatially different substructures with different functions within each tissue class in the human brain. For instance, the cortex, caudate, and putamen are anatomically different substructures in the brain, but they all belong to gray matter (GM). Due to the inherent regional differences in imaging-related properties across substructures, the intensities in different substructures, even in the same tissue class, are also more or less different. Consequently, these global methods have difficulties in the presence of intensity inhomogeneity and intensity diversification in one same tissue. In this paper, we use traditional Gaussian distribution

$$p_{i,y}(\tilde{I}(x)) = \frac{1}{\sqrt{2\pi}\sigma_{i,y}} \exp\left(-\frac{(\tilde{I}(x)-u_i(y))^2}{2\sigma_{i,y}^2}\right)$$

where u_i , s_i are local intensity means and standard deviations, respectively. Then, the ultimate goal is to minimize

$$\mathcal{E}_{local} = \int_{\Omega} \sum_{i=1}^N \int_{\Omega_i} -\omega(x-y) \log p_{i,y}(\tilde{I}(x) - \tilde{B}(y)) dx dy$$

Energy minimization in level set framework

In this paper, we consider the case of $N=2$, the multi-phase case can be solved with a similar procedure. In this case, the image domain is partitioned into two regions corresponding

to the object and background. We assume that these two regions can be represented by the regions separated by the zero level contour of function f . By using a Heaviside function H , the energy E local in the following equation can be expressed as

$$\mathcal{E}_{local} = - \int \sum_{i=1}^N \left[\int \omega(x-y) \log p_{i,y}(\tilde{I}(x) - \tilde{B}(y)) M_i(\phi(x)) dx \right] dy$$

The gradient flow

When $N=2$, the image domain is partitioned into two regions corresponding to the object and background. We assume that these two regions can be represented by the regions separated by the zero level contour of function f , the equation can be written as

$$\tilde{B}(y) = \frac{\sum_{i=1}^N \lambda_i \int \omega(x-y) \frac{|\tilde{I}(x) - u_i(y)|}{\sigma_i^2(y)} M_i(\phi) dx}{\sum_{i=1}^N \lambda_i \int \omega(x-y) \frac{1}{\sigma_i^2(y)} M_i(\phi) dx}$$

In numerical implementation, at each iteration, according to the equation, the variables u and s are updated according to the following procedure. For Fixed f and B , we find an optimal u that minimizes E .

Proposed Architecture diagram

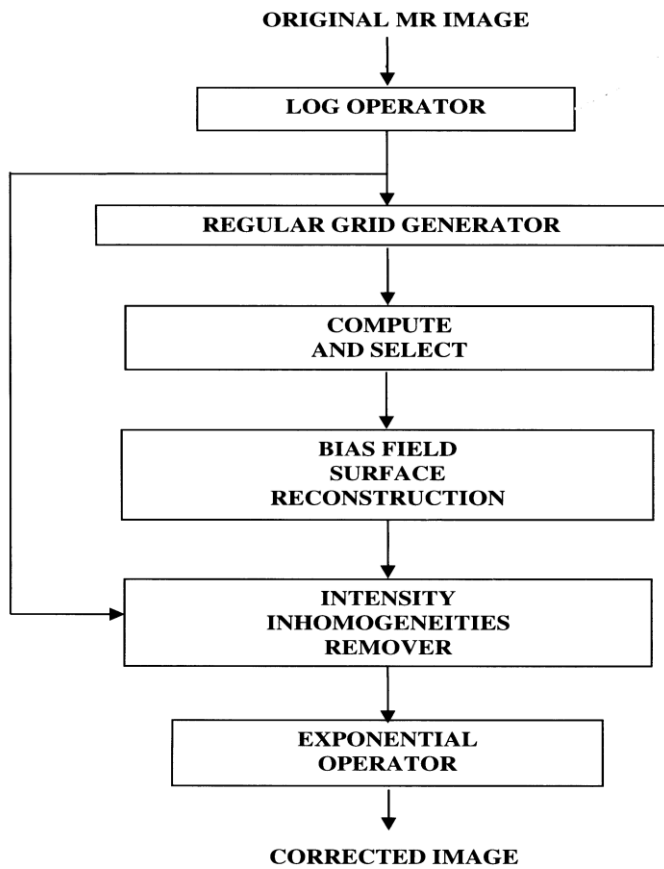


Fig: proposed Architecture diagram

V. EXPERIMENT RESULT

The programming language used with MATLAB is usually referred to as MATLAB script or M-script. After becoming familiar with the basic syntax of the M-script, a number of useful utilities are available to you that allow you to make extended uses of MATLAB. You can, for example, write programs that involve simulation. You can also create graphics, web pages, and GUI applications. When you develop programs using MATLAB, you can output the results to a number of media, including graphics files, HTML pages, PDF files, and Word documents. You can also connect up MATLAB with other applications, such as Excel or LabView to make extended uses of it. Since it is programmed in part using Java, you can modify it in the background using Java. The feasibility of the project is analyzed in this phase and business proposal is put forth with a very general plan

for the project and some cost estimates. During system analysis the feasibility study of the proposed system is to be carried out. This is to ensure that the proposed system is not a burden to the company. For feasibility analysis, some understanding of the major requirements for the system is essential.

SCREENSHOTS

5.1 INPUT IMAGE

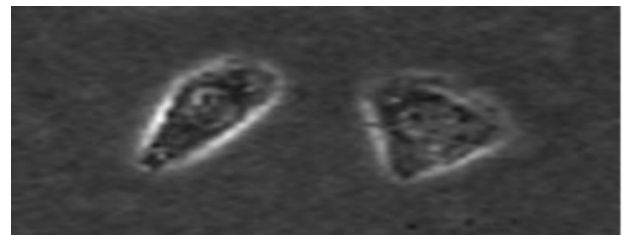


Fig 5.1 Two cell image for segmentation



Fig 5.2 CT scan image for segmentation

IMAGE SEGMENTATION FOR BRAIN TUMOR (MRI)

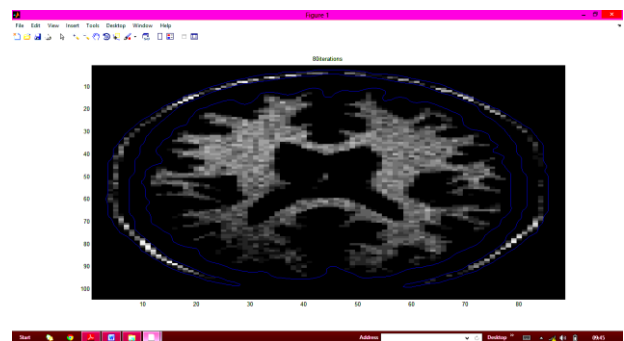


Fig 5.3 Brain Tumor in MRI

IMAGE SEGMENTATION FOR BRAIN TUMOR CT

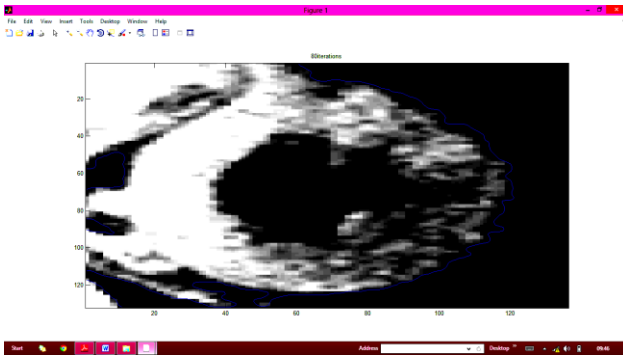


Fig 5.4 Brain Tumor in CT

IMAGE SEGMENTATION FOR MAMMOGRAM IMAGES



Fig 5.5 Mammogram Images

CLUSTER POINT MATCHING SEQUENCE (BEFORE)

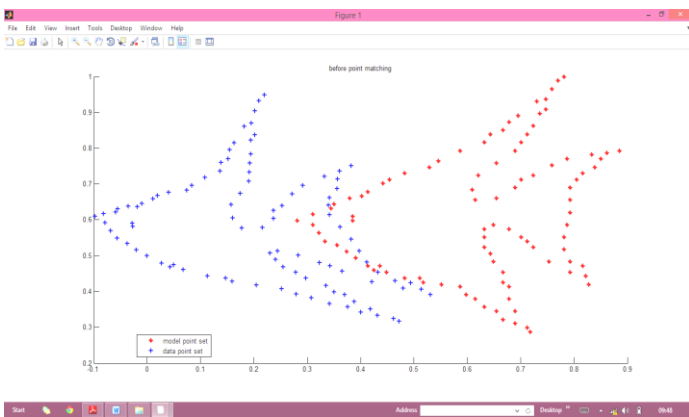


Fig 5.6 Cluster Point Matching Sequence

CLUSTER POINT MATCHING SEQUENCE (AFTER)

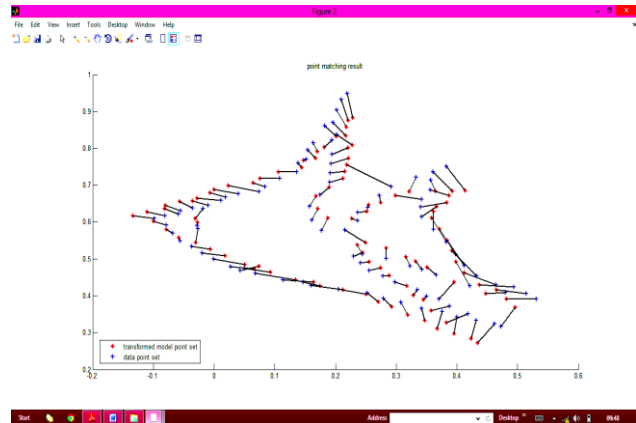


Fig 5.7 Cluster Point Matching Sequence (after)

VI. CONCLUSION

6.1 CONCLUSION

In this paper, we propose a new region-based active contour model in a variational level set formulation for bias correction and segmentation. We define an energy functional with a local intensity fitting term, which is dominant near object boundaries and responsible for attracting the contour toward object boundaries. Our model can estimate intensity inhomogeneity, handle noise efficiently, and also allows flexible initialization. Another advantage of our method is that it can be applied to some texture images in which the texture patterns can be distinguished from the local intensity variance. In addition, the regularity of the level set function is intrinsically preserved by the level set regularization term to ensure an accurate computation avoiding expensive reinitialization procedures. Comparison with some of the popular methods proves the effectiveness of our approach over standard applications.

6.2 FUTURE WORKS

In order to show the increased robustness of our method against noise, we compared our method to LBF method on simulated MR images from BrainWeb with different noise. The first column shows the initial images with the parameters: noise level 3%, noise level 5% and noise level 7%, respectively, from up to down. All these three images have inhomogeneities level 100%. The second and third columns show the results of our method and LBF method, respectively. The right column shows the ground truth. From the results, we can find our method that can obtain more satisfied results.

REFERENCE

- [1] M. Jungke, W. Seelen, G. Bielke, M. Grigat, P. Pfannenstiel, A system for the diagnostic use of tissue characterizing parameters in NMR-tomography, in: Information Processing in Medical Imaging, 1987, pp. 471–481.
- [2] U. Vovk, F. Pernus, B. Likar, A review of methods for correction of intensity inhomogeneity in MRI, IEEE Trans. Med. Imag. 26 (3) (2007) 405–421.
- [3] G. Collewet, A. Davenel, C. Toussaint, S. Akoka, Correction of intensity nonuniformity in spin-echo t1-weighted images, Magn. Reson. Imag. 20 (4) (2002) 365–373.
- [4] M. Tincher, C. Meyer, R. Gupta, D. Williams, Polynomial modeling and reduction of RF body coil spatial inhomogeneity in MRI, IEEE Trans. Med. Imag. 12 (2) (1993) 361–365.
- [5] B. Brinkmann, A. Manduca, R. Robb, Optimized homomorphic unsharp masking for MR grayscale inhomogeneity correction, IEEE Trans. Med. Imag. 17 (2) (1998) 161–171.
- [6] E. Vokurka, N. Thacker, A. Jackson, A fast model independent method for automatic correction of intensity nonuniformity in MRI data, J. Magn. Reson. Imag. 10 (4) (1999) 550–562.
- [7] K. Leemput, F. Maes, D. Vandermeulen, Automated model-based bias field correction of MR images of the brain, IEEE Trans. Med. Imag. 18 (10) (1999) 885–896.
- [8] M. Styner, C. Brechbuhler, G. Szckely, Parametric estimate of intensity inhomogeneities applied to MRI, IEEE Trans. Med. Imag. 19 (3) (2000) 153–165.
- [9] J. Ashburner, K. Friston, Voxel-based morphometry: the methods, Neuro Image 11 (6) (2000) 805–821.
- [10] J. Mangin, Entropy minimization for automatic correction of intensity nonuniformity, in: IEEE Workshop Mathematical Methods in Biomedical Image Analysis, pp. 162–169, 2000.
- [11] S. Cohen, M.Z.R.M. DuBois, Rapid and effective correction of RF inhomogeneity for high field magnetic resonance imaging, Hum. Brain Mapp. 10 (4) (2000) 204–211.
- [12] C. Han, C.Y.T.S. Hatsukami, A multi-scale method for automatic correction of intensity nonuniformity in MR images, J. Magn. Reson. Imag. 13 (3) (2001) 428–436.
- [13] J. Marroquin, B. Vemuri, S. Botello, An accurate and efficient Bayesian method for automatic segmentation of brain MRI, IEEE Trans. Med. Imag. 21 (8) (2002) 934–945.
- [14] A. Liew, H. Yan, An adaptive spatial fuzzy clustering algorithm for 3-D MR image segmentation, IEEE Trans. Med. Imag. 22 (9) (2003) 1063–1075.
- [15] O. Salvado, C. Hillenbrand, S. Zhang, MR signal inhomogeneity correction for visual and computerized atherosclerosis lesion assessment, in: 2004 IEEE International Symposium on Biomedical Imaging, 2004, pp. 1143–1146.
- [16] C. Li, C. Xu, A.W. Anderson, J.C. Gore, MRI tissue classification and bias field estimation based on coherent local intensity clustering: a unified energy minimization framework, in: Information Processing in Medical Imaging, 2009, pp. 510–519.
- [17] C. Li, C. Gatenby, L. Wang, J.C. Gore, A robust parametric method for bias field estimation and segmentation of MR images, in: CVPR, 2009, pp. 218–223.
- [18] C. Li, F. Li, C. Kao, C. Xu, Image segmentation with simultaneous illumination and reflectance estimation: an energy minimization approach, in: ICCV, 2009, pp. 702–708.
- [19] Y. Chen, J. Zhang, J. Macione, An improved level set method for brain MR images segmentation and bias correction, Comput. Med. Imag. Graphics 33 (7) (2009) 510–519.
- [20] W. Wells, W. Grimson, R. Kikinis, Adaptive segmentation of MRI data, IEEE Trans. Med. Imag. 15 (4) (1996) 429–442.
- [21] R. Guillemaud, M. Brady, Estimating the bias field of MR images, IEEE Trans. Med. Imag. 16 (3) (1997) 238–251.
- [22] J. Rajapakse, F. Kruggel, Segmentation of MR images with intensity inhomogeneities, Image Vis. Comput. 16 (3) (1998) 165–180.
- [23] Y. Zhang, M. Brady, S. Smith, Segmentation of brain MR images through a hidden Markov random field model and the expectation-maximization algorithm, IEEE Trans. Magn. 20 (1) (2001) 45–57.



[24] D. Pham, J. Prince, Adaptive fuzzy segmentation of magnetic resonance images, IEEE Trans. Med. Imag. 18 (9) (1999) 737-752.

[25] Vijayakumar, B., and Ashish Chaturvedi. "Automatic Brain Tumors Segmentation of MR Images using Fluid Vector Flow and Support Vector Machine." Research Journal of Information Technology 4.

[26] Vijayakumar, B., and Ashish Chaturvedi. "Tumor Cut-Segmentation and Classification of MR Images using Texture Features and Feed Forward Neural Networks." European Journal of Scientific Research 85.3 (2012): 363-372

[27] Vijayakumar, B., and Ashish Chaturvedi, "Idiosyncrasy Dissection and Assorting of Brain MR Images Instigating Kernel Corroborated Support Vector Machine," *Archive Des Science*

[28] Vijayakumar, B., and Ashish Chaturvedi, "Abnormality segmentation and classification of brain MR images using Kernel based Support vector machine," *Archive Des Science*, Volume 66, Issue 4.

[29] B. Vijayakumar, Ashish Chaturvedi and K. Muthu Kumar, Brain Tumor in Three Dimenesional Magnetic

Resonance Images and Concavity Analysis, International Journal of Computer Application, Issue 3, Volume 1 (February 2013)

[30] B. Vijayakumar, Ashish Chaturvedi and K. Muthu Kumar, Effective Classification of Anaplastic Neoplasm in Huddling Stain Image by Fuzzy Clustering Method, International Journal of Scientific Research, Issue 3 volume 2, March-April 2013,.

BIOGRAPHIES

E.Gajendran research scholer from sunrise university, rajasthan, india. Received the M.E. Network engineering from Anna University Coimbatore 2009. His current research interests include Data mining, image processing, bio informatics & information security.

J.Vignesh research scholer from sunrise university, rajasthan, india. Received the M.E. degree Computer science & engineering from Sathyabama University Chennai 2008. His current research interests include image processing, bio informatics & information security.

